Available online at www.sciencedirect.com
ScienceDirect
Journal of Constructional Steel Research 64 (2008) 493–504
JOURNAL OF CONSTRUCTIONAL STEEL RESEARCH
www.elsevier.com/locate/jcsr

Experimental behaviour of steel reduced beam section to concrete-filled circular hollow section column connections

Wen-Da Wang[a,b], Lin-Hai Han[a,c,*], Brian Uy[d]

[a] *Department of Civil Engineering, Tsinghua University, Beijing, 100084, China*
[b] *College of Civil Engineering, Lanzhou University of Technology, Lanzhou, 730050, China*
[c] *Department of Civil Engineering, Monash University, Clayton, VIC 3168, Australia*
[d] *School of Engineering, University of Western Sydney, Penrith South DC, NSW 1797, Australia*

Received 16 August 2007; accepted 6 October 2007

Abstract

In this paper, five specimens of connections of reduced beam section (RBS) steel beam to concrete-filled steel tubular (CFST) circular hollow section (CHS) column using an external ring were tested. The experiments considered the hysteretic behaviour under combined constant axial load and cyclic lateral load. For comparison, three specimens of a weak-column without an RBS configuration steel beam to CFST column connection were tested under the same conditions. The axial load level of the CFST column, width of connection stiffening ring and RBS configuration were considered as the experimental parameters of their seismic behaviour. It was found that the lateral load (P) versus lateral deformation (Δ) hysteresis curves exhibited no obvious strength deterioration and stiffness degradation. The energy dissipation of the RBS connections is significantly improved when compared with weak-column connections. The concrete filled CHS columns failed as a weak-column connection and their energy dissipation capacity was reduced. It can be concluded that the RBS connections exhibit good seismic performance.

Keywords: Concrete; Connections; Ductility; Energy dissipation; Reduced beam section (RBS); Seismic behaviour; Steel; Steel beam

1. Introduction

In a real building structure, connections play a key role for a structure in determining whether or not a structure will reach its theoretical ultimate load, because plastic hinges are usually formed at the location of two or more members.

A conventional type of moment-resisting connection, which consists of a concrete-filled steel tubular (CFST) column and a steel beam, shown in Fig. 1, is widely used in tall buildings and has been investigated by a large number of researchers (e.g. Alostaz and Schneider [1]; Azizinamini and Schneider [2]; Schneider and Alostaz [3]). However, in practice in China, it was found that the ring width of this type of connection designed according to the regulations of the Japanese Code AIJ [4] or the Chinese Code DBJ13-51-2003 [5] is too large to be adopted, because it is difficult to incorporate the large ring plate, particularly for CFST columns with a sectional size exceeding 500 mm. A reasonable width of the outside ring of this type of connection is of concern to engineers. Thus, a smaller dimension of the connection is desirable and advantageous for construction [6].

The reduced beam section (RBS) moment connection for structural steel was based on the recommended configuration of the AISC *Seismic Provisions for Structural Steel Buildings* [7]. In a reduced beam section (RBS) moment connection, portions of the beam flanges are selectively trimmed in the region adjacent to the beam-to-column connection. In an RBS connection, yielding and hinge formation are intended to occur primarily within the reduced section of the beam, and thereby limit the moment and inelastic deformation demands developed at the face of the column [8]. A review of the research literature indicates that a large number of RBS connections have been tested under a variety of conditions by different investigators at institutions throughout the world, such as Chambers et al. [9], Chen et al. [10], Chen and Chao [11], Jin et al. [12], etc.

* Corresponding author at: Department of Civil Engineering, Tsinghua University, Beijing, 100084, China. Tel.: +86 10 62797067; fax: +86 10 62781488.
E-mail addresses: wdwang@tsinghua.edu.cn (W.-D. Wang), lhhan@tsinghua.edu.cn (L.-H. Han), b.uy@uws.edu.au (B. Uy).

0143-974X/$ - see front matter © 2007 Elsevier Ltd. All rights reserved.
doi:10.1016/j.jcsr.2007.10.005

Notations

A_s	Steel cross-sectional area
A_c	Concrete cross-sectional area
b_f	Overall width of I-beam
D	Sectional dimension of steel tube
E	Dissipated energy ability
E_c	Concrete modulus of elasticity
E_s	Steel modulus of elasticity
f_{cu}	Concrete cube strength
f_{sy}	Yield strength of steel
f_u	Ultimate strength of steel
h	Overall height of I-beam
h_e	Equivalent damping coefficient
H	Height of column of the connection
k	Beam to column linear stiffness ratio
K_j	Lateral rigidity of connection
L	Length of beam of connection
n	Axial load level ($n = N_0/N_u$)
N_0	Axial load of CFST column
N_u	Ultimate compressive resistance of CFST column
P	Lateral load of connection
P_u	Estimated ultimate lateral load capacity of connection
P_{ue}	Ultimate lateral load capacity of connection by experiment
P_y	Yield lateral load capacity of connection
SCC	Self-Consolidating Concrete
t_f	Flange thickness of I-beam
t_s	Wall thickness of the steel tube
t_w	Web thickness of I-beam
α	Steel ratio ($\alpha = A_s/A_c$)
ε_y	Yield strain
ν_s	Poisson's ratio of steel
ν_c	Poisson's ratio of concrete
Δ	Lateral displacement of connection
Δ_y	Yield displacement of connection
Δ_u	Lateral displacement when lateral load of connection falls to 85% of P_{ue}
μ	Displacement ductility coefficient

A significant amount of testing on RBS connections was also conducted under the FEMA/SAC program [13]. Most RBS connection test specimens of structural steel have been tested pseudo-statically, using a loading protocol in which applied displacements are progressively increased, such as the loading protocol specified in ATC-24 [14]. However, few RBS beam to CFST column connections have been tested under pseudo-static loading.

This paper provides new test data pertaining to the behaviour of steel RBS beam to CFST column connections using an external ring. Each connection was modeled as an internal joint from a planar frame. The eight connection specimens with circular cross-sections were tested under a constant axial load and a cyclically increasing flexural load. Five RBS connections to CFST columns were tested and three normal connections

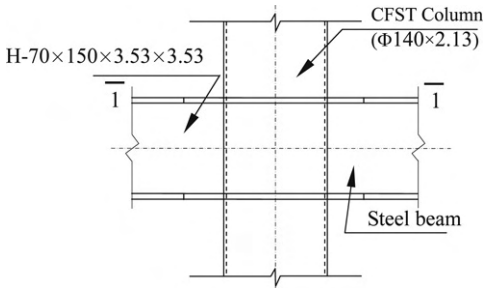

(a) Connection elevation.

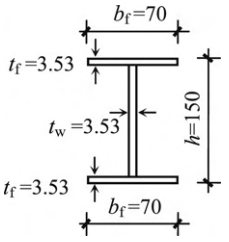

(b) Section of steel beam.

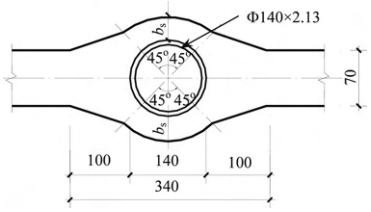

(c) Section 1-1 for CJ-21, CJ-22, CJ-33.

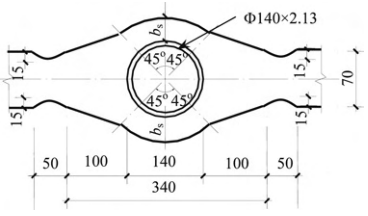

(d) Section 1-1 for CJ-13N, CJ-21N, CJ-22N, CJ-23N, CJ-33N.

Fig. 1. Connection configuration (Unit: mm).

with weak-column specimens were considered for comparison. The test parameters included the width of ring, the axial load level and the configuration of the RBS. There were three types of connection specimens used to compare their mechanical performance for different ring widths. It was shown that the energy dissipation capacity of RBS connections are much improved, when compared with the weak-column connections. The axial load level of the column has an effect on the strength and seismic behaviour of the connections. With an increase in the axial load level of the column, the lateral ultimate strength of the connections reduces, and the displacement ductility and the capacity of energy dissipation also reduce. It can be concluded that the RBS to CFST column connection has reasonable seismic performance. The work in this paper provides a basis for further development of a theoretical model, which will be described in another paper, and will help to establish an approach to calculate the strength and overall behaviour of these types of connections.

2. Experimental program

2.1. General

Eight connection specimens of steel beam to CFST column using an external ring with circular cross-section, were tested

Table 1
Summary of connection specimen information

Specimen number	Specimen size (mm)			Width of ring (mm)	N_0 (kN)	Axial load level n	P_{ue} (kN)	Δ_y (mm)	Total energy dissipation E (kN m)	μ
	Specimen section		Length							
CJ-21	Column	$\Phi 140 \times 2.13$	1050	40	40	0.05	35.48	14.57	13.70	4.58
	Beam	$150 \times 70 \times 3.53 \times 3.53$	1500							
CJ-22	Column	$\Phi 140 \times 2.13$	1050	40	265	0.3	37.67	10.53	13.35	4.12
	Beam	$150 \times 70 \times 3.53 \times 3.53$	1500							
CJ-33	Column	$\Phi 140 \times 2.13$	1050	20	530	0.6	35.94	7.69	23.52	6.93
	Beam	$150 \times 70 \times 3.53 \times 3.53$	1500							
CJ-13N	Column	$\Phi 140 \times 2.13$	1050	60	530	0.6	39.40	7.62	43.46	7.25
	Beam	$150 \times 70 \times 3.53 \times 3.53$	1500							
CJ-21N	Column	$\Phi 140 \times 2.13$	1050	40	40	0.05	35.06	10.92	12.72	3.81
	Beam	$150 \times 70 \times 3.53 \times 3.53$	1500							
CJ-22N	Column	$\Phi 140 \times 2.13$	1050	40	265	0.3	38.93	13.88	25.55	3.85
	Beam	$150 \times 70 \times 3.53 \times 3.53$	1500							
CJ-23N	Column	$\Phi 140 \times 2.13$	1050	40	530	0.6	38.30	9.16	31.91	5.98
	Beam	$150 \times 70 \times 3.53 \times 3.53$	1500							
CJ-33N	Column	$\Phi 140 \times 2.13$	1050	20	530	0.6	32.48	6.63	24.23	7.09
	Beam	$150 \times 70 \times 3.53 \times 3.53$	1500							

Note: Beam's section parameters means $h \times b_f \times t_w \times t_f$, and column's section means $D \times t_s$.

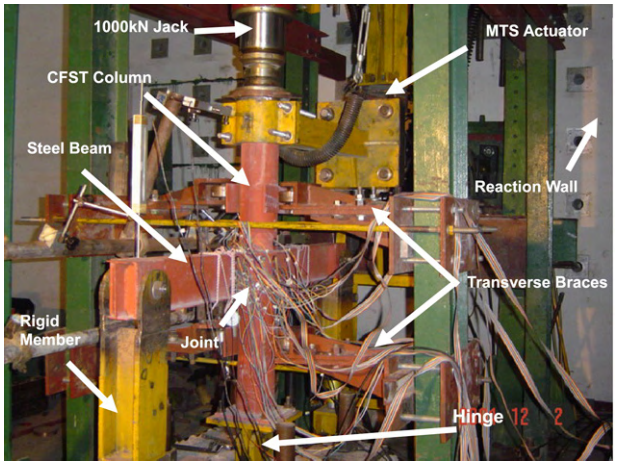

Fig. 2. Arrangement of test set-up.

under a constant axial load and a cyclically increasing lateral load. Fig. 2 shows the test setup. The column height was 1050 mm, and the steel beam span was 1500 mm. Five RBS specimens were designed with strong-column–weak-beam behaviour, so that the beam failure mode could be predicted. The other three connections were designed to exhibit strong-beam–weak-column behaviour and the steel beam did not have an RBS section, and thus the dominant column failure mode resulted. The test specimens were designed to investigate the effects of changing the following parameters:

- The width of the external ring: there were three types of rings according to their width. The width of the ring, which was predicted by the Japanese Code AIJ [4] or the Chinese specification DBJ13-51-2003 [5] was type I, and those with two-thirds and one-third of the width were type II and type III, respectively;
- The axial load level of the CFST column, n (= 0.05, 0.3 and 0.6), which is defined as $n = N_0/N_u$, where N_0 is the axial load applied in the column and N_u is the axial compressive capacity of the column and N_u was determined by Eurocode 4 [15];
- The beam configuration, five specimens included RBS beam connections and the other three had normal connections.

Table 1 lists the details of each connection specimen, respectively, where h, b_f, t_w, and t_f are the overall height, overall width, web thickness and flange thickness of the I-beam respectively; D and t_s are the overall dimension and thickness of the circular steel tube respectively. Table 1 also provides the width of the ring, the axial load N_0 and axial load level n for the CFST columns. The calculated nominal strength N_u was calculated by using the mechanics model described in the specification for CFST structures Eurocode 4 [15] and using the recorded steel and concrete mechanical properties given in Table 2.

The circular hollow sections were manufactured with cold-formed steel tubes. The ends of the steel tube sections were cut and machined to the required length. The steel beams and the external ring had the same thickness as the beam. The upper and lower flanges of the ring were made from the same steel sheet. These were manufactured from mild steel sheet, with three plates being cut from the sheet, tack welded into an I-shaped cross-section and then welded with a single bevel-butt weld at the corners. The ring plates and the web of the I-beam were welded to the steel tube. All welded seams were 3 mm in thickness. Fig. 1 provides detailed dimensions of the typical test connection respectively.

Each steel tube was welded to a circular steel base plate of 12 mm thickness. The specimens were placed upright to air-dry until heating. During curing, a very small amount of

Table 2
Material properties of steel

Steel type	t (mm)	f_{sy} (N/mm^2)	f_u (N/mm^2)	E_s (N/mm^2)	ν_s
CHS tube	2.13	272.3	350.6	2.06×10^5	0.278
Steel beam and ring	3.53	289.0	431.0	2.04×10^5	0.262

longitudinal shrinkage of 0.7–0.9 mm or so occurred at the top of the column. High-strength concrete was used to fill this longitudinal gap at the end so that the concrete surface was flush with the steel tube at the top.

2.2. Material properties

Strips of the steel tubes and sheets (cut from the beams) were tested under tension. Three coupons, which were extracted from each face of the steel tube and the steel beam respectively, were tested to determine their yield strength (f_{sy}), ultimate strength (f_u), modulus of elasticity (E_s) and Poisson's ratio (ν_s). If there is an obvious plastic yielding point, such as in the steel beam, the yield strength is determined from the recorded stress–strain curve corresponding to the plastic yielding point. If there is no obvious plastic yielding point, such as in the material of the CHS tubes, the yield strength is determined corresponding to the point with a residual strain of 0.2%. The measured average yield strength (f_{sy}), ultimate strength (f_u), modulus of elasticity (E_s) and Poisson's ratio (ν_s) are summarised in Table 2.

The SCC (Self-Consolidating Concrete) mix was designed for a compressive cube strength (f_{cu}) at 28 days of approximately 52.6 N/mm^2 for the connection specimens. The modulus of elasticity (E_c) of the concrete was measured, the average value being 41,500 N/mm^2. The mix proportions were as follows:

- Cement: 300 kg/m^3
- Blast furnace slag: 200 kg/m^3
- Water: 181 kg/m^3
- Sand: 994 kg/m^3
- Coarse aggregate: 720 kg/m^3
- Additional high-range water reducer (HRWR): 2.4 kg/m^3

The fresh properties of the SCC mixture were given as follows:

- Slump flow (mm): 262
- Fresh air content (%): 4.5
- Unit weight (kg/m^3): 2397
- Concrete temperature (°C): 28
- Flow time (s): 14
- Flow speed (mm/s): 57
- Flow distance (mm): 610

The average concrete cube strength of each specimen at the time of the test was 60.0 N/mm^2. The SCC was poured without any vibration.

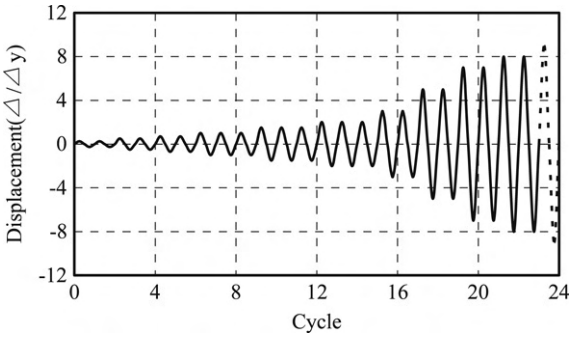

Fig. 3. Typical loading history.

2.3. Cyclic loading apparatus

Fig. 2 provides a schematic view of the beam–column connection test setup. The lateral load was applied at the top of the CFST column. To facilitate loading and to prevent local failure of the specimen under the loading point, a very rigid stub made of high strength steel was connected firmly to the top part of the column as shown in Fig. 2. The stub was made of two separate halves of a box with a concentric hole that fit exactly within the column end. The two halves were pushed against the specimen and connected together using six high strength bolts. The stub was attached to an MTS hydraulic ram with a 500 kN capacity. The ends of the connection specimen were attached to cylindrical bearings and were free to rotate in-plane, and thus simulating pinned end conditions.

2.4. Loading history

The lateral loading history of the connection was generally based on the ATC-24 [14] guidelines for cyclic testing of structural steel components. The loading history included elastic cycles and inelastic cycles. Because the lateral loading capacities of the specimens were very small, it was considered unsafe to conduct the loading by load control. Instead, the elastic cycles were conducted under displacement control at displacement levels of $0.25\Delta_y$, $0.5\Delta_y$ and $0.7\Delta_y$, where Δ_y is the estimated lateral yielding displacement corresponding to the lateral yielding load P_y, which is equal to $0.7P_u$ approximately, where P_u is the estimated ultimate lateral loading capacity, which is calculated using the mechanics model developed by Wang [16]. Two cycles were imposed at each of the lateral displacement levels of 0.25, 0.5 and $0.7\Delta_y$. The inelastic cycles were then taken to lateral displacement levels of Δ_y, $1.5\Delta_y$, $2\Delta_y$, $3\Delta_y$, $5\Delta_y$, $7\Delta_y$ and $8\Delta_y$. Three cycles were imposed at each displacement level of Δ_y, $1.5\Delta_y$ and $2\Delta_y$; two cycles were imposed at each additional inelastic displacement level described above. The adopted loading history is shown in Fig. 3.

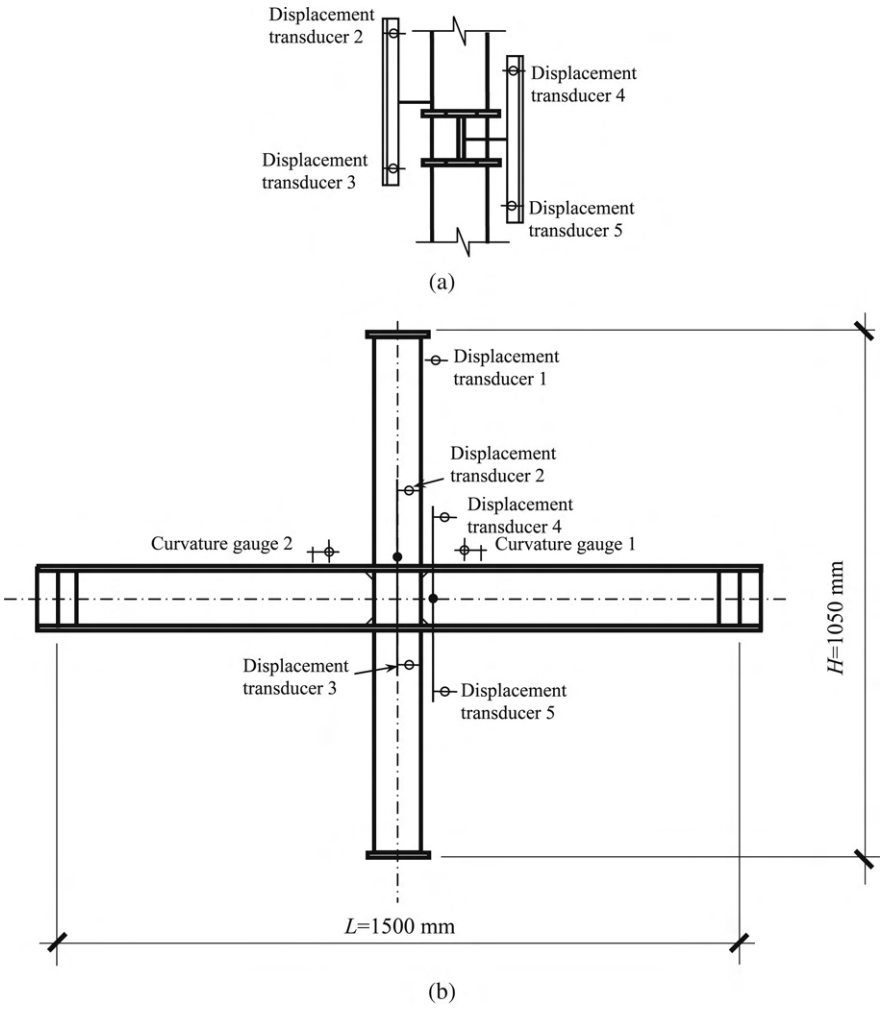

Fig. 4. Arrangement of displacement transducers.

2.5. Measurements

The in-plane displacements were measured by five displacement transducers at locations along the connection specimen as shown in Fig. 4. Displacement transducer 1 was used to measure the displacement at the top of the column at the load application point of the MTS hydraulic ram. The other four displacement transducers were used to obtain rotations at the beam end and column end of the connection core as shown in Fig. 4. Two curvature gauges were used to measure the curvatures of the steel beam close to the external ring. Strain gauges were also used to measure the strains in the steel beam, the steel tube of the connection core and the steel plate of the external ring. The axial load (N_0) of columns was applied and held constant by a 1000 kN hydraulic ram. The hydraulic pump was fixed to the sliding support, as shown in Fig. 2, which allowed the specimen to move freely in-plane and ensure that the column axial load was always concentric. Precautions were made to avoid any eccentricity in the axial load application by very careful alignment of the test setup.

3. Experimental observations and failure modes

All of the RBS test connection specimens behaved in a ductile manner and the test proceeded in a smooth and controlled fashion. It was found that, most of the RBS specimens except CJ-21N, after the steel reached 2.3–4.2 ε_y (yield strain), local yielding occurred at the beam compression flanges close to the exterior ring on both sides of the column. With increasing lateral displacement, the beam webs also experienced local yielding, and then the complete section of the beam buckled to develop a plastic hinge. It can be concluded that the specimens failed in a strong-column–weak-beam mode. For the normal beam section with weak-column connections, such as CJ-21, CJ-22, CJ-33, they exhibited significant deformation at the column near the joint panel at first, and the column finally failed by bearing. The deformation of the steel beam was fairly insignificant during the test. It can be concluded that those specimens failed in a strong-beam–weak-column mode. Specimen CJ-33 and RBS connection CJ-33N had the smallest width ring, and the ring failed when the lateral load bearing reached the maximum value because the strength of the ring was insufficient, whilst the beam flange and web had no obvious deformation. For the test specimen CJ-33, failure occurred by column cracking. However, for specimen CJ-33N for failure with a beam plastic hinge through their rings was partly the cause of failure. Specimen CJ-21N failed as a weak-column connection because the axial load level was 0.05, and the ultimate moment capacity of the column was less than

(a) CJ-21 ($n = 0.05$). (b) CJ-22 ($n = 0.3$). (c) CJ-33 ($n = 0.6$). (d) CJ-13N ($n = 0.6$).

(e) CJ-21N ($n = 0.05$). (f) CJ-22N ($n = 0.3$). (g) CJ-23N ($n = 0.6$). (h) CJ-33N ($n = 0.6$).

Fig. 5. Failure modes of specimens.

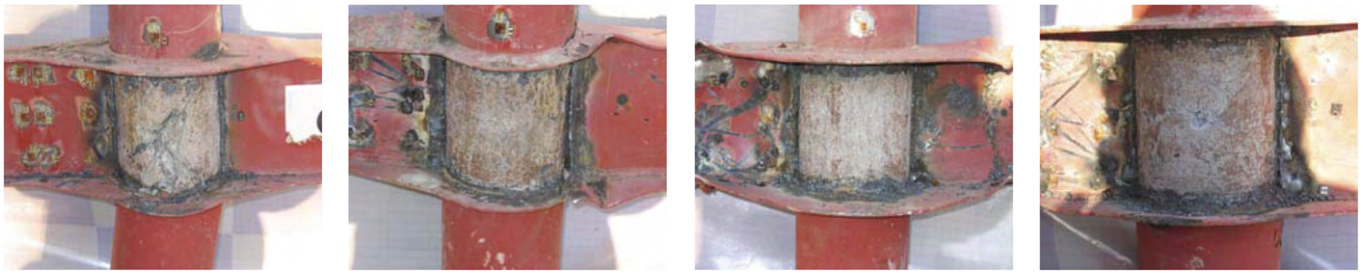

(a) CJ-21. (b) CJ-33. (c) CJ-13N. (d) CJ-23N.

Fig. 6. Failure modes of core concrete at connection panel.

the ultimate moment capacity of the RBS beam, though it is an RBS connection. The welding between the steel beam and the steel tube for all of the connections was in good condition, after the testing, and there was no obvious fracture found.

The failure modes of those connections were varied for the different test parameters. There are three kinds of failure modes in general according to the beam configuration. The failure mode was mainly dependent on the width of the ring and the RBS configuration. Fig. 5(a)–(h) shows all the failure modes of the connection specimens after the tests, respectively. The three failure modes which occurred, are: the RBS beam failure, occurred in CJ-13N, CJ-22N, CJ-23N, CJ-33N; the column failure, occurred in CJ-21, CJ-22, CJ-21N; and the column and ring failure, occurred in CJ-33. Typical failure modes of the core concrete at the connection panel are compared in Fig. 6(a)–(d), respectively. It was found that the damage of the core concrete of CJ-21 was fairly evident, but the concrete of the other connections remained in good condition.

4. Test results and discussion

4.1. Test results

The recorded curves of lateral load (P) versus lateral displacement (Δ) at the top of the column (Fig. 2) for all connections are shown in Fig. 7. The test results show that the lateral load (P) versus lateral displacement (Δ) hysteretic curves of the RBS connections except for CJ-21N specimen are of a "plump shape" in general. The curves illustrate no obvious strength deterioration and stiffness degradation. The tested RBS connections exhibited an improved seismic behaviour in general. The load (P) versus displacement (Δ) hysteretic curves of the weak-column connection specimens, such as CJ-21, CJ-22, CJ-33 and CJ-21N, exhibited a noticeable pinching effect. The stiffness upon reloading of all the connections gradually decreased with the incremental lateral displacement while the stiffness upon unloading was similar to the initial elastic stiffness, and it was similar to the initial stiffness. The moment and curvature of the CFST column sections were increased with the incremental lateral displacement.

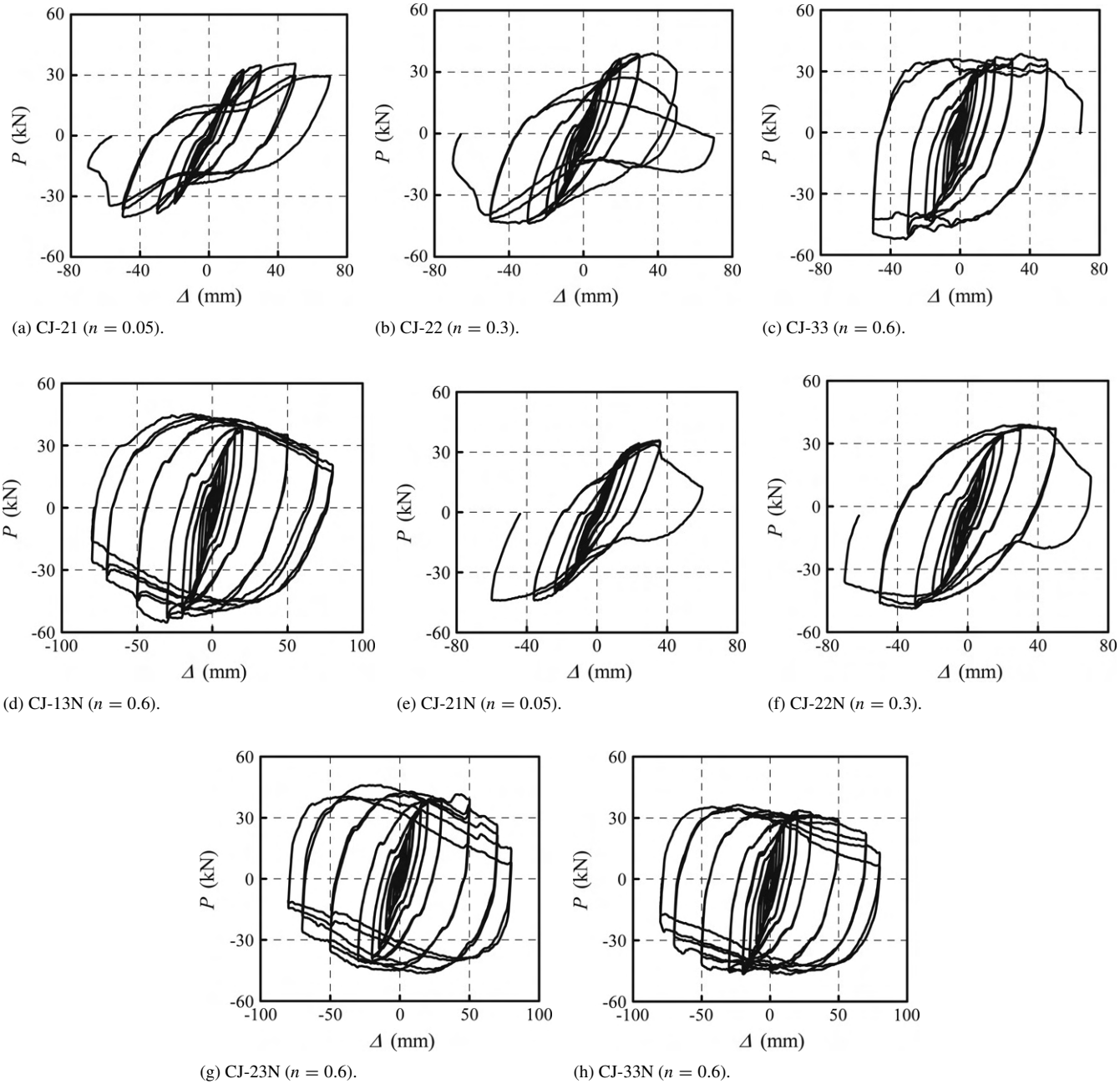

(a) CJ-21 ($n = 0.05$). (b) CJ-22 ($n = 0.3$). (c) CJ-33 ($n = 0.6$).

(d) CJ-13N ($n = 0.6$). (e) CJ-21N ($n = 0.05$). (f) CJ-22N ($n = 0.3$).

(g) CJ-23N ($n = 0.6$). (h) CJ-33N ($n = 0.6$).

Fig. 7. Lateral load (P) versus displacement (Δ) hysteretic curves.

The recorded curves of lateral load (P) versus lateral displacement (Δ) envelope curves of the connections are shown in Fig. 8(a)–(c) under different parameters, respectively. The maximum loads (P_{ue}) obtained from the curves, are shown in Table 1. The ultimate load and ductility of the connections decreased with an increment of axial load level for the same ring width, such as CJ-22N and CJ-23N, as well as CJ-33 and CJ-33N, from Fig. 8(a) and (b), respectively. The ultimate load of the RBS connections descended with the reduced width of the ring at the same axial load level from Fig. 8(c).

The lateral load versus lateral displacement relation of connections may be converted to provide the column bending moment versus relative beam–column rotation in the column at the column to top beam flange intersection. The bending moment may be calculated as:

$$M_j = P \cdot (H/2 - h/2) + N_0 \cdot (\delta_u - \delta_m), \quad (1)$$

where δ_u is the horizontal displacement at the top of the column, δ_m is the horizontal displacement at the column end of the connection panel, H and h are the column and beam heights respectively.

The relative rotation (θ) may be taken as the difference in global rotations of the beam and the column, being obtained respectively by the displacements measured at the beam ends and the column ends divided by the distances between the respective ends. Specimen CJ-21 and CJ-22N were used to

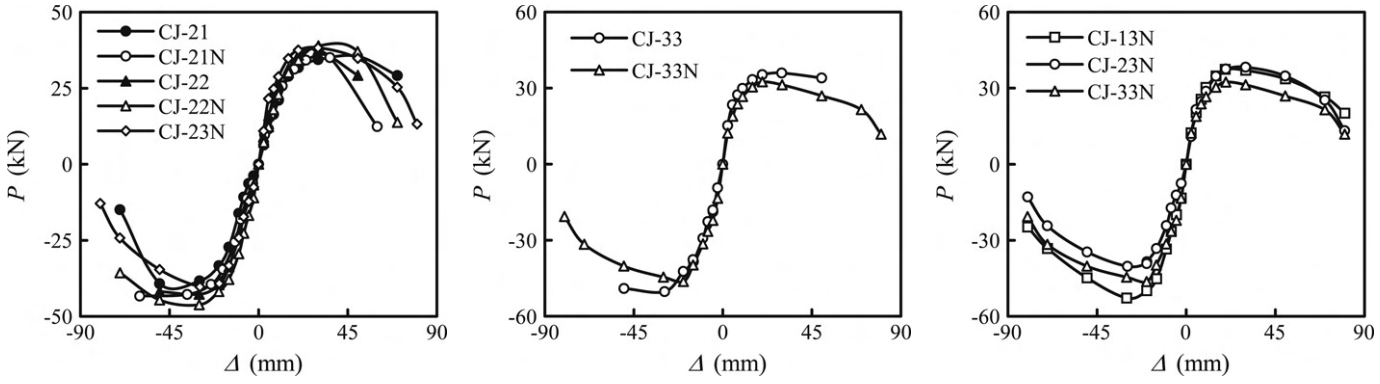

(a) The same width of ring. (b) Different beam configuration. (c) Different axial load level.

Fig. 8. Lateral load (P) versus displacement (Δ) envelope curves.

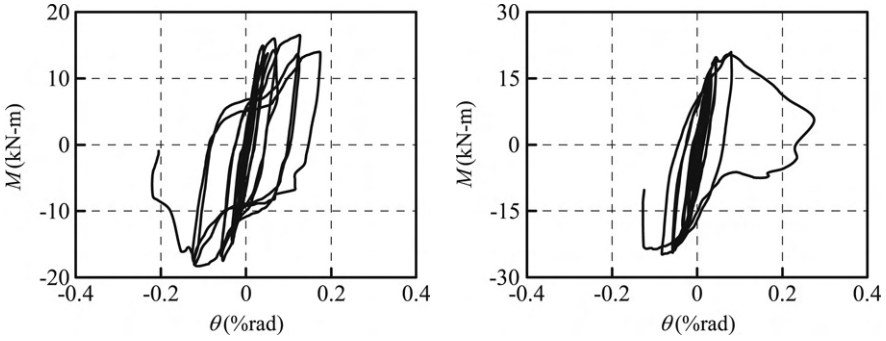

(a) CJ-21. (b) CJ-22N.

Fig. 9. Typical moment (M) versus relative rotation (θ) hysteretic curves of beam end.

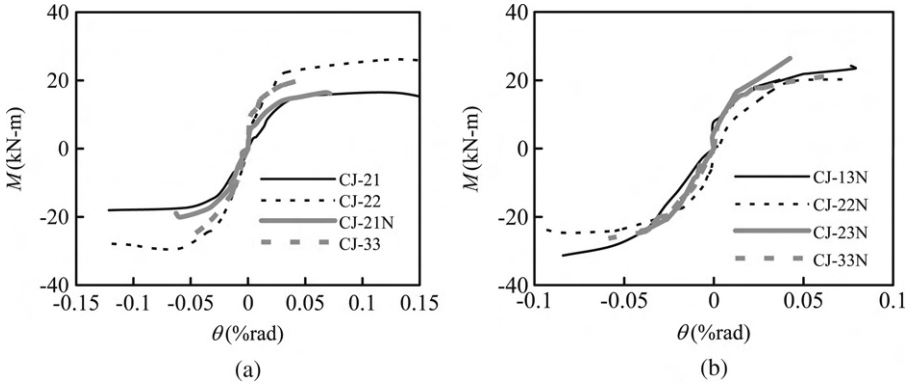

Fig. 10. Moment (M) versus relative rotation (θ) envelope curves of beam end.

demonstrate the typical response of the measured moment (M) versus relative beam–column rotation (θ) graph as shown in Fig. 9(a) and (b) respectively. It can be seen that there is an initial elastic response, followed by inelastic behaviour with gradually decreasing stiffness, until the ultimate bending moment capacity of the connection is reached asymptotically. The moment (M) versus relative beam–column rotation (θ) envelope curves of all connections are shown in Fig. 10(a) and (b) respectively. The relative beam–column rotation of weak-column connections was larger than the RBS connections except for CJ-21N because the large bending deformation of the weak-column induces larger rotations.

Fig. 11 shows a typical recorded moment (M) versus curvature (ϕ) curve for the beam of those connections. The moment (M) versus curvature (ϕ) curve envelope curves of all connections are shown in Fig. 12(a) and (b) respectively. The recorded moment (M) was obtained by multiplying the force, which was measured by the load cell, by the span between the supporting point and steel beam end. It can be seen that the steel beam of the RBS connections exhibited good hysteretic behaviour of resistance to cyclic bending, especially the post-buckling behaviour. In contrast, the weak-column connections had similar deformation capacity, and the steel beam exhibited no obvious buckling and deformation during the test.

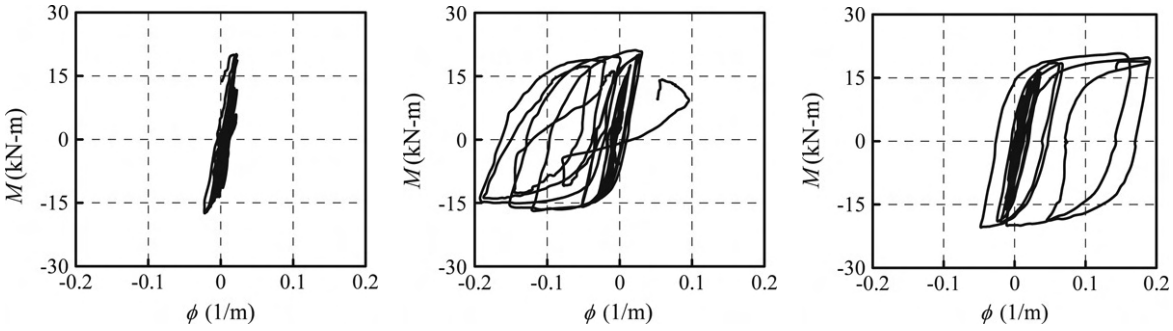

(a) CJ-22. (b) CJ-13N. (c) CJ-22N.

Fig. 11. Typical moment (M) versus curvature (ϕ) hysteretic curves of beam end.

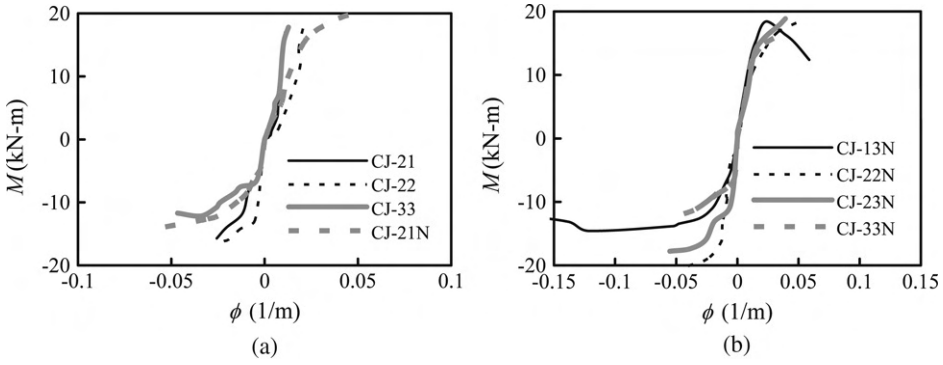

Fig. 12. Moment (M) versus curvature (ϕ) envelope curves of beam end.

4.2. Effects of different test parameters on connection behaviour

4.2.1. Effects of axial load level

Table 1 shows the measured ultimate load (P_{ue}) of all connections. The yielding load of connections was determined according to Fig. 13. Fig. 8(a) shows that the axial load level (n) not only influences the ultimate lateral load, but also the ductility of the specimen. Whilst the ultimate lateral load is only slightly reduced at a higher axial load level, the ductility of the specimen at a higher load level is much lower for connections as shown in Table 1. Here ductility is measured by the ductility coefficient $\mu(= \frac{\Delta_u}{\Delta_y})$, where Δ_y is the lateral displacement at material yield and Δ_u is the lateral displacement when the lateral load falls to 85% of the maximum lateral strength. The RBS connections had an improved ductility compared with the other three weak-column connections in general.

The recorded lateral load to deflection relationship may be simplified as shown in Fig. 14. From this simplification, Eq. (2) may be used to calculate the equivalent damping coefficient (h_e) according to Tang [17], which has been adopted in the Chinese standard JGJ 101-96 [18] also. In Eq. (2) S_{ABC} and S_{CDA} are areas under curve ABC and CDA shown in Fig. 14(a) respectively, and S_{OBE} and S_{ODF} are areas within triangles OBE and ODF shown in Fig. 14(b) respectively.

$$h_e = \frac{1}{2\pi}\frac{S_{ABC} + S_{CDA}}{S_{OBE} + S_{ODF}}. \quad (2)$$

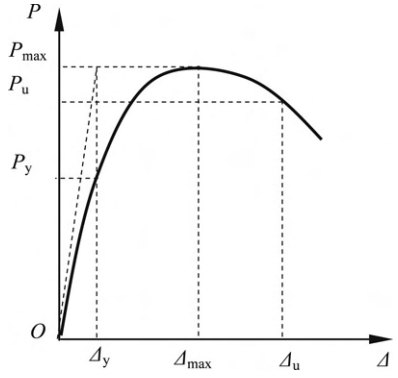

Fig. 13. Determination for yield point of specimens.

Fig. 15 demonstrates that the cumulative equivalent damping coefficient (h_e) of connections increases greatly with increasing relative displacement (Δ/Δ_y). The axial load level has some effect on the h_e–(Δ/Δ_y) relationship, with a higher axial load level tending to obviously increase the equivalent damping coefficient for the connections.

Fig. 16 shows the effect of axial load level on rigidity degradation of the specimen as a function of the relative lateral displacement (Δ/Δ_y). The rigidity (K_j) is expressed as $K_j = \frac{\sum_{i=1}^{m} P_j^i}{\sum_{i=1}^{m} u_j^i}$, where P_j^i and u_j^i are the maximum load and lateral displacement respectively, under the ith loading cycle when the relative lateral displacement (Δ/Δ_y) equals j, and m is the cycle time of loading. It can be concluded that increasing

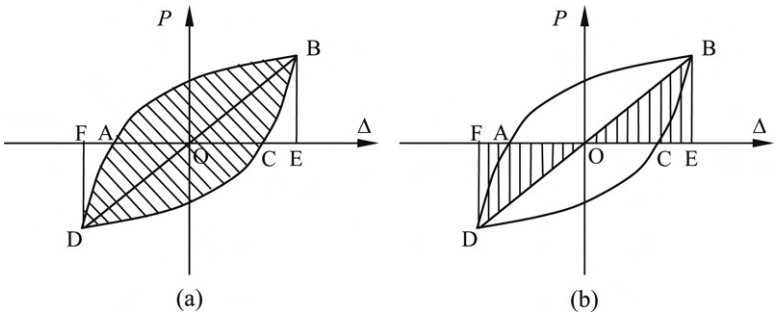

Fig. 14. Idealized P–Δ hysteretic relationship.

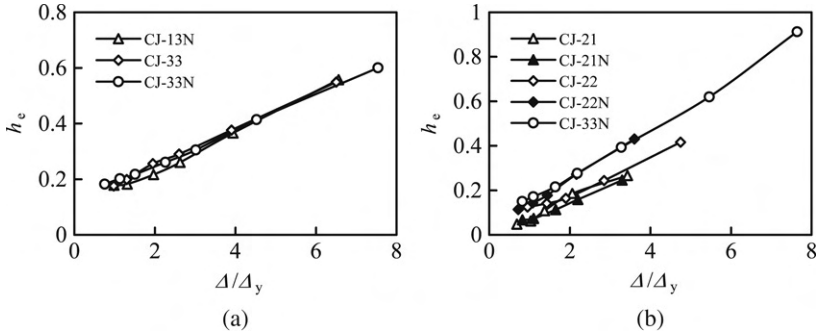

Fig. 15. h_c–Δ/Δ_y curves.

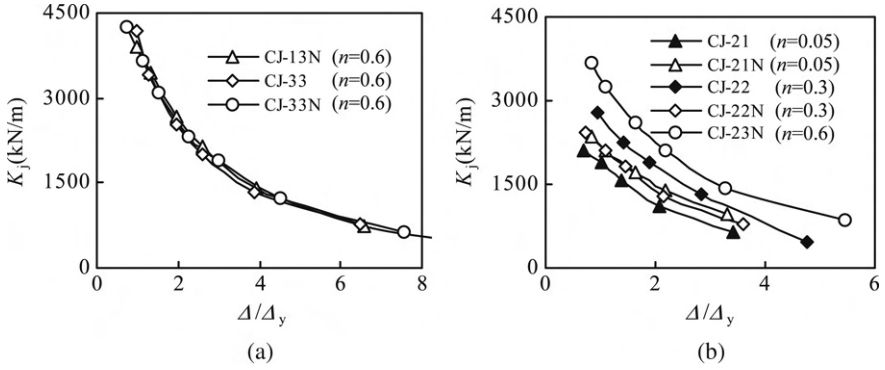

Fig. 16. Rigidity degradation curves.

the axial load level significantly reduces the rigidity for the connections.

4.2.2. *Effects of ring width*

The width of the ring had an influential effect on the ultimate strength (P_{ue}) of the connection. Fig. 8(c) shows the relationship between the ring width with respect to the ultimate bearing capacity which reduces with decreasing ring width. There were different failure modes of the two types of connections. The plastic hinge location of the RBS connections was moved from the beam end to the connection between the column and the ring, and the failure mode changed from a plastic hinge on the beam end to cracking of the ring, as shown in Fig. 5, respectively.

4.2.3. *Effects of RBS configuration*

Fig. 8(a) and (b) shows the influence of the RBS configuration on the lateral load (P) and ductility of the connections. It was found that, generally, the ultimate lateral load (P_{ue}) decreases slightly with an RBS beam, such as CJ-33 and CJ-33N in Fig. 8(b), however the ductility of the specimen improves for an RBS connection.

4.3. *Dissipated energy and rigidity degradation*

Table 1 illustrates the total dissipated energy capability of the connection specimens and Fig. 15 provides the relationship between the equivalent damping coefficient (h_e) and the relative displacement (Δ/Δ_y). The equivalent damping coefficient (h_e) is determined according to Eq. (2). The dissipated energy capability (E) of every hysteretic loop described in Fig. 11 should be calculated as:

$$E = 2\pi h_e. \tag{3}$$

As expected, Table 1 indicates that: (1) In general, the axial load level had a slight influence on the total dissipated

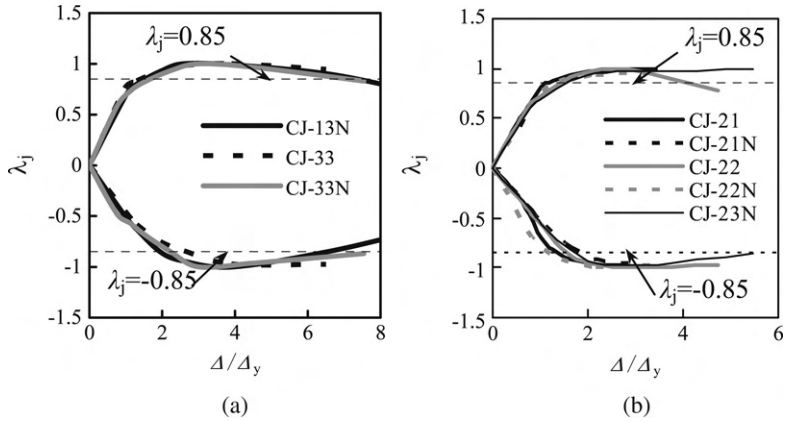

Fig. 17. Strength deterioration curves.

energy ability (E) of the specimens; (2) The RBS connections had a much better total dissipated energy capability than the weak-column connections. Fig. 15 and Table 1 demonstrate that the equivalent damping coefficient (h_e) increases quickly with the increasing relative displacement (Δ/Δ_y) under higher axial load level for connections because of the higher energy obtained by a higher axial load.

Fig. 16 shows the rigidity degradation of the specimen versus the relative displacement (Δ/Δ_y) relationship curves. It can be seen from Fig. 16 that the axial load level has an obvious influence on the $K_j - (\Delta/\Delta_y)$ curves of the connections, i.e. K_j degrades sharply with increasing relative displacement (Δ/Δ_y) under higher axial load level for the connections.

Fig. 17 shows the strength degradation of the connections versus the relative displacement (Δ/Δ_y) relationship curves. The strength degradation coefficient λ_j is defined by the maximum load of every cyclic load loop divided by the ultimate load (P_{ue}). It can be seen that the strength degradation of all connections was not evident in general. The distinct strength degradation occurred after (Δ/Δ_y) was equal to 4. The strength degradation of RBS connections was much greater than the weak-column connections.

5. Conclusions

This paper has described a series of new tests for RBS steel beam to concrete filled steel tubular (CFST) column connections using an external ring and has presented a discussion on the effects of different test parameters (axial load level, width of ring and beam configuration) on the following characteristics of column and connection performance: lateral ultimate strength, ductility, energy dissipation, damping coefficient and rigidity degradation. From the results of this paper, the following conclusions may be drawn:

(1) The RBS beam to CFST column connections were designed based on the weak-beam–strong-column approach. All the RBS connections observed a failure mode of beam failure in general. In contrast, the weak-column connections failed in a brittle mode. The RBS connections exhibited good seismic performance and ductility whilst the ultimate load may be reduced slightly.

(2) At a higher axial load level in the column, the column lateral load carrying capacity is slightly reduced, but its ductility suffered a large reduction. As a result, the energy dissipation is also greatly reduced. The damping coefficient is only slightly increased. Initially, there is a slight increase in the column lateral rigidity at low deflections, but the degradation in column lateral rigidity is much greater at large lateral deflections.

(3) The ultimate load of the connections was decreased with a decreasing width of the ring of the connections, and the ring failure mode occurred under the same axial load level and beam configuration.

Acknowledgements

The research reported in the paper is a part of the Project 50425823 supported by the National Natural Science Foundation of China, and the project supported by the Start-Up Fund for Outstanding Incoming Researchers of Tsinghua University. Their financial support is highly appreciated. The authors also wish to thank Mr. You Jin-Tuan for his assistance in the test program. The authors would also like to acknowledge the support of the University of Western Sydney International Research Initiatives Scheme which has supported the collaboration between Professor Han and Professor Uy at the Universities of Tsinghua and Western Sydney respectively.

References

[1] Alostaz YM, Schneider SP. Analytical behaviour of connections to concrete-filled steel tubes. Journal of Constructional Steel Research 1996; 40(2):95–127.

[2] Azizinamini A, Schneider SP. Moment connections to circular concrete-filled steel tube columns. Journal of Structural Engineering ASCE 2004; 130(2):213–22.

[3] Schneider SP, Alostaz YM. Experimental behaviour of connections to concrete-filled steel tubes. Journal of Constructional Steel Research 1998; 45(3):321–52.

[4] AIJ. Recommendations for design and construction of concrete filled steel tubular structures. Tokyo (Japan): Architectural Institute of Japan (AIJ); 1997.

[5] DBJ13-51-2003. Technical specification for concrete-filled steel tubular structures. 2003 [in Chinese].

[6] You JT, Chen GD, Han LH. Preliminary discussion on the dimension of ring of concrete-filled steel tube column joint with external ring. Journal of Harbin Institute of Technology 2005;37(Supp):354–7 [in Chinese].
[7] AISC/ANSI 341-05. Seismic provisions for structural steel buildings. Chicago (IL): American Institute of Steel Construction, Inc.; 2005.
[8] AISC/ANSI 358-05. Prequalified connections for special and intermediate steel moment frames for seismic applications specification. Chicago (IL): American Institute of Steel Construction, Inc.; 2005.
[9] Chambers JJ, Almudhafer S, Stenger F. Effect of reduced beam section frames elements on stiffness of moment frames. Journal of Structural Engineering 2003;129(3):383–93.
[10] Chen SJ, Yeh CH, Chu JM. Ductile steel beam-to-column connections for seismic resistance. Journal of Structural Engineering 1996;122(11): 1292–9.
[11] Chen SJ, Chao YC. Effect of composite action on seismic performance of steel moment connections with reduced beam sections. Journal of Constructional Steel Research 2001;57(4):417–34.
[12] Jin J, El-Tawil S. Seismic performance of steel frames with reduced beam section connections. Journal of Constructional Steel Research 2005;61(4): 453–71.
[13] FEMA 355D. State of the art report on connection performance. Prepared by the SAC Joint Venture for the Federal Emergency Management Agency. Washington, DC; 2000.
[14] ATC-24. Guidelines for cyclic seismic testing of components of steel structures. Redwood City (CA): Applied Technology Council; 1992.
[15] CEN. Eurocode 4: Design of composite steel and concrete structures. Part 1.1, General rules and rules for buildings (EN 1994-1-1:2004). 2004.
[16] Wang WD. Behaviour of steel beam to concrete-filled steel tubular columns frames. Ph.D. thesis of Fuzhou University, China, 2006 [in Chinese].
[17] Tang JR. Seismic performance of reinforced concrete frame connection. Nanjing: Southeast University Press; 1989 [in Chinese].
[18] JGJ101-96. Specification for test methods of seismic buildings. Beijing: Architecture Industrial Press of China; 1997 [in Chinese].